

ALFALFA HI Data Stacking III. Comparison of environmental trends in HI gas mass fraction and specific star formation rate

Silvia Fabello^{1*}, Guinevere Kauffmann^{1†}, Barbara Catinella¹, Cheng Li²,
Riccardo Giovanelli³, Martha P. Haynes³

¹Max-Planck Institut für Astrophysik, D-85741 Garching, Germany

²Max-Planck-Institute Partner Group, Shanghai Astronomical Observatory, Nandan Road 80, Shanghai 200030, China

³Centre for Radiophysics and Space Research, Cornell University, Ithaca, NY 14853, USA

28 October 2018

ABSTRACT

It is well known that both the star formation rate and the cold gas content of a galaxy depend on the local density out to distances of a few Megaparsecs. In this paper, we *compare* the environmental density dependence of the atomic gas mass fractions of nearby galaxies with the density dependence of their central and global specific star formation rates. We stack HI line spectra extracted from the Arecibo Legacy Fast ALFA survey centered on galaxies with UV imaging from GALEX and optical imaging/spectroscopy from SDSS. We use these stacked spectra to evaluate the mean atomic gas mass fraction of galaxies in bins of stellar mass and local density. For galaxies with stellar masses less than $10^{10.5} M_{\odot}$, the decline in mean atomic gas mass fraction with density is stronger than the decline in mean global and central specific star formation rate. The same conclusion does not hold for more massive galaxies. We interpret our results as evidence for ram-pressure stripping of atomic gas from the outer disks of low mass satellite galaxies. We compare our results with the semi-analytic recipes of Guo et al. (2011) implemented on the Millennium II simulation. These models assume that only the diffuse gas surrounding satellite galaxies is stripped, a process that is often termed “strangulation”. We show that these models predict relative trends in atomic gas and star formation that are in disagreement with observations. We use mock catalogues generated from the simulation to predict the halo masses of the HI-deficient galaxies in our sample. We conclude that ram-pressure stripping is likely to become effective in dark matter halos with masses greater than $10^{13} M_{\odot}$.

Key words: galaxies: evolution – galaxies: ISM – radio lines: galaxies

INTRODUCTION

Systematic studies of the dependence of galaxy properties on environment began with analyses of the relation between galaxy morphology and local density (Oemler 1974; Dressler 1980). It later became evident that star formation is more strongly affected by environment than morphology (Hashimoto et al. 1998). Large surveys, for example the Sloan Digital Sky Survey (SDSS; York et al. 2000) and the Two-degree Field Galaxy Redshift Survey (2dFGRS; Colless et al. 2001) provided samples large enough to study the ef-

fects of local galaxy density on a multiplicity of galaxy properties. It was shown that the star formation and structural properties of galaxies depend strongly on their mass (e.g. Kauffmann et al. 2003; Shen et al. 2003; Baldry et al. 2004). Because of this, and because galaxy mass is itself correlated with environment, it is important to bin galaxies by mass before studying how their properties vary with local density. Several analyses showed that at fixed mass, the dependence of colour/star formation on density is stronger than that of structural properties such as concentration index and stellar surface mass density (Kauffmann et al. 2004; Li et al. 2006a; Bamford et al. 2009; Skibba et al. 2009). This suggests that environmentally-driven processes lead to cessation of star

* fabello.silvia@gmail.com

† gamk@mpa-garching.mpg.de

formation in a galaxy, but do not strongly affect its structure.

An alternative way of quantifying environmental effects is to study how the properties of galaxies vary as a function of distance from the centers of groups and clusters. The “center” is usually defined as the position of the brightest galaxy in the system and the distance is usually scaled to the virial radius. One result that has emerged from such studies is that at fixed clustercentric distance, galaxy properties do not depend strongly on the mass of the group (Balogh et al. 2004; Van den Bosch et al. 2008). This does not agree with a scenario in which the ram-pressure effects are responsible for removing the cold interstellar medium in galaxies and shutting down star formation. Ram-pressure depends on the square of the velocity at which a galaxy is moving through the surrounding gas, so it should operate more efficiently in galaxies in more massive dark matter halos.

In 1980, Larson, Tinsley & Caldwell suggested that the gas *envelopes* surrounding disks are most easily stripped by ram-pressure effects when they fall into a cluster. After a few Gyr, the galaxy will have converted its available cold gas into stars and because there is no infall of new gas, the galaxy will “starve” and stop forming stars. This mechanism has long been part of semi-analytic models of galaxy formation (e.g. Kauffmann et al. 1993). In recent years, the predictions of these models have been compared with data from SDSS and it has been found that the fraction of red satellites is *higher* in the models than in the data (Kimm et al. 2009; Weinmann et al. 2010). Star formation quenching timescales must therefore be quite long (2-3 Gyr) in satellite galaxies (Wang et al. 2007). In the optical astronomy community, “slow gas starvation” has thus come to be accepted as the main physical process determining how galaxies evolve in dense environments.

We note, however, that optical studies present a biased picture of how environment affects galaxies. In disk galaxies, atomic gas generally extends to substantially larger radii than the stars. Ram-pressure will act primarily on low density atomic gas in the outer regions of galaxies, rather than the dense molecular gas in their central regions. The first systematic studies of the dependence of the atomic gas content of galaxies on environment (Haynes, Giovanelli & Chincarini 1984; Giovanelli & Haynes 1985; Gavazzi 1987) found that disk galaxies in clusters exhibit a deficiency in HI content that strongly increases towards the cluster centre and that matches the predictions of the the ram-pressure stripping model introduced by Gunn & Gott (1972). Integrated CO observations of cluster galaxies suggested that there is no deficiency of molecular gas in HI-deficient galaxies (Kenney & Young 1989), but resolved studies showed some evidence of CO depletion when the HI is stripped to within the optical disk (Vollmer et al. 2008; Fumagalli et al. 2009). Both results support the idea that ram-pressure stripping primarily affects gas in the outer regions of galaxies, proceeding inward. Subsequent work by Gavazzi (1989), Cayatte et al. (1990), Kenney, Van Gorkom & Vollmer (2004), Chung et al. (2009) emphasized the frequent presence of cluster galaxies with truncated HI disks which, together with examples of disturbed HI morphologies and one-side tails, also support the mechanism of ram-pressure. Finally, SPH simulations (Abadi, Moore & Bower 1999; Vollmer 2009) of galaxies orbiting through the intra-cluster medium then demonstrated

that ram-pressure can in fact be responsible for distorted HI disks similar to those seen in the observations.

The degree to which ram-pressure may affect the interstellar medium of galaxies outside the rich cluster environment is not yet well understood. Available samples have generally been too small to quantify environmental effects across a large dynamic range in local density or dark matter halo mass. The state-of-the-art blind HI survey, the Arecibo Legacy Fast ALFA survey (ALFALFA; Giovanelli et al. 2005), does detect HI in galaxies in environments spanning a range of environments from voids to rich clusters, but ALFALFA is still a shallow survey so it will only detect gas-rich galaxies at redshifts greater than ~ 0.02 . In this paper, we employ the stacking technique described in Fabello et al. (2011a, hereafter Paper I) to study the *average* cold gas content of galaxies as a function of local density for a sample of ~ 5000 galaxies with redshifts in the range $0.025 < z < 0.05$. By comparing the variation of the HI gas fraction with environment with the variation of their total and central specific star formation rates, we aim to constrain the environments in which ram-pressure stripping effects become important. As we have discussed, ram-pressure stripping will preferentially affect the low density outer disks of galaxies, which are dominated by atomic gas where star formation is inefficient (Bigiel et al. 2010).

We begin by describing the data and the density estimator that we use in this analysis. We then compare the *relative* decrease in HI gas fraction and specific star formation rate as a function of local density and compare our results with the results of semi-analytic models implemented on the Millennium II Simulation (Boylan-Kolchin et al. 2009). Discussion and conclusions are presented in the final section.

1 THE SAMPLE

Our galaxies are selected from the “parent sample” of the GALEX Arecibo SDSS Survey (Catinella et al. 2010), which is a volume-limited sample of ~ 12000 galaxies selected from the SDSS main spectroscopic sample with stellar masses greater than $10^{10} M_{\odot}$ and redshifts in the range $0.025 < z < 0.05$, and which lie in the intersection of the footprints of the SDSS Data Release 6 (Adelman-McCarthy et al. 2008), the GALEX Medium Imaging Survey (Martin et al. 2005) and the ALFALFA survey. We make use of *sample A* defined in Paper I, which consists of 4726 galaxies in the ALFALFA 40% dataset (Haynes et al. 2011). Only 23% of *sample A* targets are detected by ALFALFA. We employ a stacking technique, which allows us to include the many non-detections. We refer the reader to Paper I for a comprehensive description of the stacking method; in this paper, we only provide a brief summary. Before proceeding, we also describe the parameters used in this analysis; these include stellar mass, global and fibre specific star formation rates (§1.2), and our adopted environmental tracer (§1.3).

1.1 ALFALFA data stacking

ALFALFA is a blind HI survey that used the ALFA multibeam receiver at the Arecibo telescope to scan 7000 deg^2 of the sky over the velocity interval $v[\text{kms}^{-1}] \simeq [-2500; 18000]$ (i.e. out to $z \sim 0.06$). The data acquired are

stored as smaller three dimensional cubes of dimension $2.4^\circ \times 2.4^\circ$ on the sky and 5500 km s^{-1} in velocity “depth”. The stacking process that we apply to ALFALFA data includes a series of steps, which can be summarized as follows:

a. Create a catalogue of HI spectra

All our targets are selected from the SDSS spectroscopic survey, so we know their position on the sky and their redshift. We select the ALFALFA data-cube which contains the target and integrate the signal from the galaxy over a sky region of $4' \times 4'$ (our targets are always smaller than the telescope beam, whose FWHM is $\sim 3.5'$). For each spectrum we measure the root mean square (*rms*) noise, which is used later as a weight.

b. Stack spectra

We co-add the signals from N different sources located at different redshifts. First, we shift each spectrum to the target galaxy rest frequency, so each spectrum is centered at zero velocity. We stack together the spectra S_i ($i=1,..N$) using their $w_i = 1/rms^2$ as a weight, so that the final spectrum S_{stack} is:

$$S_{stack} = \frac{\sum_{i=0}^N S_i \cdot w_i}{\sum_{i=0}^N w_i}. \quad (1.1)$$

If we recover a signal in the stacked spectrum, we measure the integrated emission between the two edges of the HI profile, which are defined manually for each spectrum. If there is no detection, we evaluate an upper limit, assuming a 5σ signal with a width of 300 km s^{-1} , smoothing the spectrum to 150 km s^{-1} .

c. Evaluate HI gas fractions

Our aim is to compute the average HI content of a given sample of galaxies, so we are interested in converting our recovered signal into an HI mass and subsequently into an average HI gas fraction. Once we measure an HI flux, we estimate the corresponding HI mass using:

$$\frac{M_{\text{HI}}}{M_\odot} = \frac{2.356 \times 10^5}{1+z} \left(\frac{D_L(z)}{\text{Mpc}} \right)^2 \left(\frac{S_{int}}{\text{Jy km s}^{-1}} \right) \quad (1.2)$$

where $D_L(z)$ is the luminosity distance and S_{int} the integrated HI flux. The HI gas fraction is simply defined as M_{HI}/M_* . Note that we weight each spectrum before stacking by $M_*^{-1}(1+z)^{-1}D_L(z)^2$, to convert it into a measure of “gas fraction” (see also the discussion in Paper I, Appendix A).

At the median redshift of *sample A*, the size of the Arecibo telescope beam corresponds to physical scales of 0.15 Mpc and may include more galaxies than the targeted one. For our gas fractions to be reliable, we apply a correction for contamination from close companions, as described in detail in Appendix A. In summary, for each galaxy which lies inside a region of the beam size $\pm 300 \text{ km s}^{-1}$ around the main target, we estimate its gas fraction from photometry using the relation between colour, stellar mass surface density and HI gas fraction found by Zhang et al. (2009), and subtract it from the HI mass of the target galaxy. The corrections are always smaller than a few percent even in the highest density bins.

1.2 Galaxy Parameters

The optical parameters we use are drawn from the MPA-JHU SDSS DR7 release of spectrum measurements or from Structured Query Language (SQL) queries to the SDSS DR7 database server¹. We use UV/optical colours derived from convolving the SDSS images to the same resolution as the GALEX images; this is described in more detail in Wang et al. (2010).

The parameters used in this paper are the following.

Stellar masses M_* are derived from SDSS photometry using the spectral energy distribution (SED) fitting technique described in Salim et al. (2007) with a Chabrier (2003) initial mass function.

Specific star formation rates (sSFR) are defined as the star formation rate per unit stellar mass, SFR/M_* [yr^{-1}]. We use two different measures of sSFR to trace different regions of the galaxies: a fibre and a global specific star formation rate. 1) The *fibre specific star formation rate* is measured inside the 3-arcsecond SDSS fiber, and is therefore characteristic of the inner regions. At the median redshift of the sample ($z = 0.035$), the 3 arcsecond diameter fiber subtends a physical length scale of 2.1 kpc . The radius enclosing 50% of the *r*-band light for galaxies with stellar masses between $10^{10} - 10^{11} M_\odot$ ranges from 2 to 3 kpc. So the fraction of the total galaxy light going down the fibre will be around 5-10%. We acquire the fibre specific star formation rates from the MPA-JHU SDSS DR7 release of spectrum measurements². Briefly, they are evaluated from the spectrum emission lines, to which a grid of photo-ionization models from Charlot & Longhetti (2001) is fitted, following the methods described in Brinchmann et al. (2004). For objects whose signal is contaminated by AGN emission or for objects with low S/N emission lines, the SFRs are derived indirectly from the 4000 \AA break strength. 2) the *global specific star formation rate* is obtained by applying a spectral energy distribution (SED) fitting technique to the five optical and two GALEX UV total flux measurements. A more thorough discussion of this procedure is presented in Sain tonge et al. (2011).

1.3 Local density estimator

Similar to other past studies of galaxy environment (e.g. Kauffmann et al. 2004; Blanton & Berlin 2007; Thomas et al. 2010), we define a density parameter for each galaxy as the number of neighbours with $\text{Log } M_* [M_\odot] \geq 9.5$ located inside a “cylindrical” aperture of 1 Mpc radius and $\pm 500 \text{ km s}^{-1}$ depth, centred on the target. Environmental effects are strongest if density is evaluated on scales comparable to the typical virial radii of the haloes hosting the galaxies in the sample. 1 Mpc is somewhat larger than the typical virial radius of haloes hosting L_* galaxies, but on smaller scales the number of tracer galaxies becomes too small and Poisson noise dominates.

We search for neighbours with $\text{Log } M_* [M_\odot] \geq 9.5$ in the MPA-JHU DR7 spectroscopic catalogue. We note that

¹ See <http://www.mpa-garching.mpg.de/SDSS/DR7/> and <http://cas.sdss.org/dr7/en/tools/search/sql.asp>

² <http://www.mpa-garching.mpg.de/SDSS/DR7/>

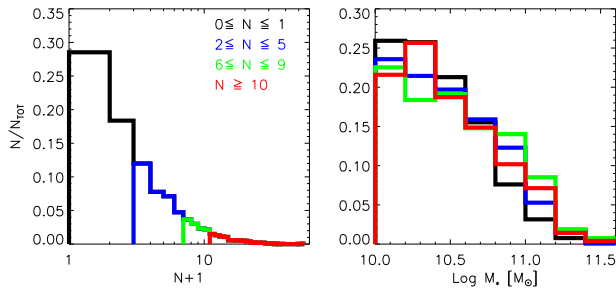


Figure 1. *Left:* normalized distribution of the density parameter N (plotted as $N+1$ for convenience). The colours indicate the four density bins we will use throughout the paper, as reported in the legend. *Right:* Normalized stellar mass distribution for galaxies in each of the density bins.

two SDSS fibres cannot be closer than 55 arcseconds, so we might miss close companions. In order to correct for this “fibre collision” effect, we follow the approach of Li et al. (2006b), who measured the angular two-point correlation function for the SDSS spectroscopic sample $[w_z(\theta)]$ and for the parent photometric sample $[w_p(\theta)]$. The ratio:

$$F(\theta) = \frac{1 + w_p(\theta)}{1 + w_z(\theta)}$$

is used to correct for the effect of fibre collisions. We adopt the correlation functions from Li et al. (2006a) and weight each neighbour by $F(\theta)$, where θ is the angular separation from the main target. In practice, fibre collision corrections on the estimate of N are very small on average ($\sim 3\%$).

The distribution of the density parameters N derived for *sample A* galaxies is shown in Figure 1, left panel (note that we actually plot $N+1$ for convenience). Just under 50% of the galaxies in our sample have zero or one neighbour. The right panel shows the normalised stellar mass distribution for galaxies with 0-1, 2-5, 6-9 and > 10 neighbours, following the colour legend in the left panel. As can be seen, the stellar mass distributions do not change very much between the different density bins. As we will show, this is because most galaxies in the bin with > 10 neighbours are not in rich cluster environments, but in dark matter halos of moderate mass ($\sim 10^{13} M_\odot$).

In Figure 2, we show the spatial distribution of galaxies found around two objects in our sample with $N > 10$. On the left, we plot the galaxies projected on the sky in units of Mpc. The target galaxies are represented by the red dots and the black circles around them indicate the physical size of the Arecibo beam at the redshift of the target. On the right, we show the three-dimensional distributions of the neighbours. The galaxy in the top row is the one with largest number of neighbours in *sample A* ($N = 72$). This galaxy lies in the far outskirts of the Coma cluster (the mean redshift of the Coma cluster is $cz = 6853 \pm 1082 \text{ km s}^{-1}$ (Colless & Dunn 1996), and this galaxy lies at $cz = 7860 \text{ km s}^{-1}$). Most of the Coma cluster is actually outside our redshift range, however. In the bottom row of Figure 2, we show a typical galaxy with $N = 17$. As can be seen, such a galaxy is not in a cluster, but in a group.

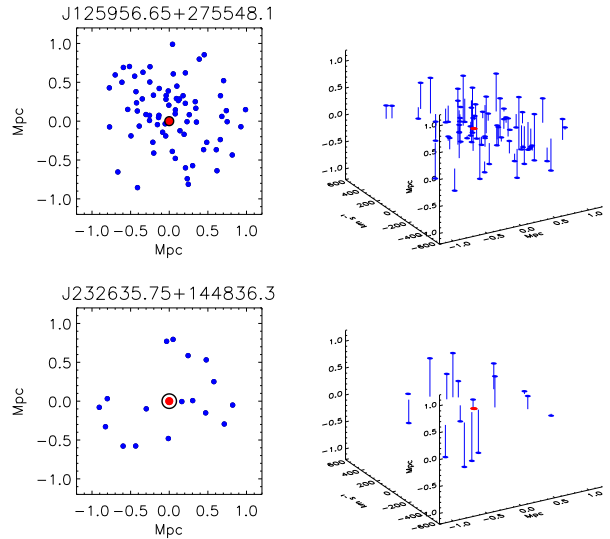


Figure 2. Sky distribution of neighbours around two galaxies in our sample. *Left:* sky projection as a function of distance (in Mpc) from the central target. The size of the Arecibo beam is overplotted as a black circles on the central galaxies (red dot, SDSS name on top). *Right:* three-dimensional view of the same group, with the redshift/velocity component added. The top row shows the galaxy in the richest environment in our sample, the bottom row a typical galaxy in the density bin with $N > 10$.

2 COMPARISON OF THE DENSITY DEPENDENCE OF HI MASS FRACTIONS AND GLOBAL/FIBRE SSFRS

It is well known that both star formation rates and HI gas fractions are smaller in galaxies in dense environments (e.g. Balogh et al. 2004; Cortese et al. 2011). As we have discussed, a *comparison* of how the HI mass fractions and the specific star formation rates of galaxies measured in their centers and in their outer regions depend on environment should constrain the physical origin of these effects. Because the atomic gas extends to larger radii and lower densities than the gas that traces the young stars, a comparison of the local density dependence of atomic gas mass fractions and central sSFRs should also provide considerable insight. In a pure starvation scenario, where there is no replenishment of the cold gas in the disk from cooling of the hot halo, we would expect the HI and the star formation to decrease at the same rate as a function of density. If ram-pressure stripping of the atomic gas is important, we would expect the HI to exhibit a stronger environmental dependence.

In this section, we compare the *relative* decrease in HI mass fraction, global and central specific star formation rates as a function of local density for galaxies in different stellar mass bins. We divide our sample (we do not consider galaxies with $M_* > 10^{11} M_\odot$ because of limited statistics) into two bins of stellar mass and four bins of local density. For each bin, we compute M_{HI}/M_* , global and fibre specific star formation rates. We then scale these values by dividing by the value measured for the lowest density bin ($0 \leq N \leq 1$) at the same stellar mass. In this way, we compare the relative decrease of each quantity with density.

Results are shown in Figure 3. The orange solid lines represent the HI gas mass fractions, the blue solid lines show

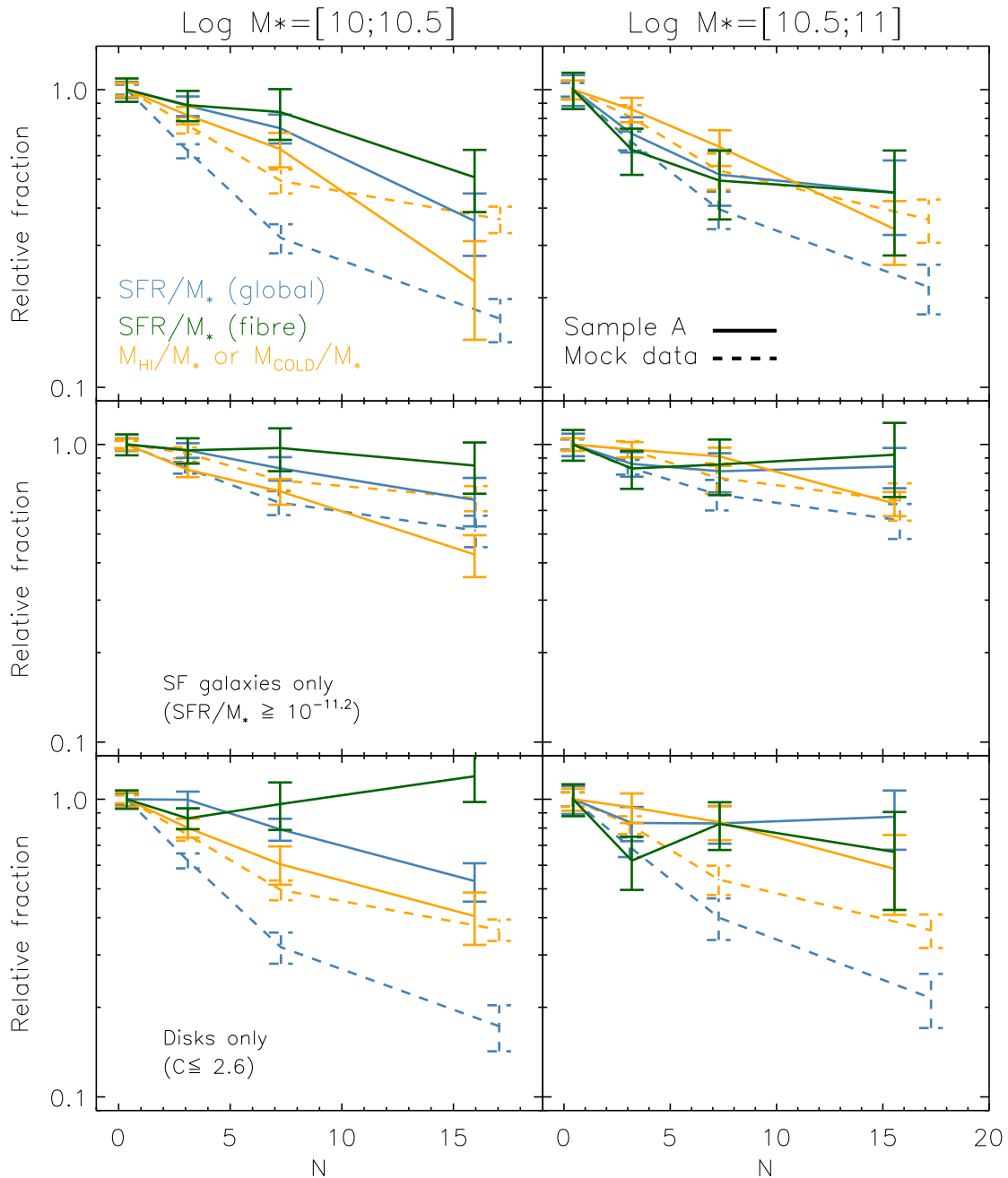


Figure 3. Comparison of the relative dependence of the H I gas fraction (orange), the global specific star formation rate (blue) and the fibre specific star formation rate (green) as a function of local density for 2 bins of M_* , as labelled at the top of the diagram. *First row:* Results are shown for all galaxies. *Second row:* Results are shown for star-forming galaxies with $\text{Log SFR}/M_* \geq -11.2$. *Third row:* Results are shown for disk-dominated galaxies with $C \leq 2.6$. Solid lines show results obtained by stacking *sample A* galaxies. Error bars are evaluated by bootstrap re-sampling the galaxies in the stack. Dashed lines show the results derived from semi-analytic model mock catalogues (see Section 2.1).

the global specific star formation rates, and the green solid lines the fibre specific star formation rates. Errorbars are computed by bootstrap resampling 80% of the galaxies included in the stacks. The dashed lines show results from models and are discussed in detail in the next section.

The top panels show results for the whole *sample A*, while the second and third panels investigate different sub-populations to gain better insight into the processes at work.

In particular, the middle row focuses on galaxies with $\text{Log SFR}/M_* [\text{yr}^{-1}] \geq -11.2$. The cut is chosen because it is the minimum of the bimodal distribution of specific star formation rates of galaxies in our sample (see von der Linden et al. 2010). The bottom panels show results for disk-dominated galaxies, selected from *sample A* to have concentration indices less than 2.6. The concentration index is defined as the ratio of the radii enclosing 90% and 50% of the r -band light

and is quite tightly correlated with the bulge-to-total ratio B/T of the galaxy (Gadotti 2009). $C < 2.6$ corresponds to $B/T < 0.3$ (see also Weinmann et al. 2009). As can be seen, for galaxies with stellar masses in the range $10 < \text{Log } M_{\star} < 10.5$, there is a clear ordering in that the HI mass fraction declines most steeply as a function of local density, followed by the global and fibre specific star formation rate. For galaxies with stellar masses in the range $10.5 < \text{Log } M_{\star} < 11$, there is no similar ordering.

As we have discussed, *sample A* does include galaxies located at the edge of the Coma cluster. In order to check the extent to which the effects seen in Figure 3 are caused by a sub-population of cluster galaxies, we exclude Coma cluster galaxies from our analysis and replot the mean gas fraction and specific star formation rate curves in Figure 4. In practice, we exclude 12 galaxies with stellar masses greater than $10^{10} M_{\odot}$ within 3 degrees and $\pm 2000 \text{ km s}^{-1}$ of the center of the Coma cluster. As can be seen, the decrease in both the average HI gas mass fraction and the global and specific star formation rates as a function of density becomes somewhat weaker when the Coma galaxies are discarded, but the ordering remains the same. As we will discuss later, our results thus support a scenario in which ram-pressure stripping affects low mass galaxies in *moderate-density environments*.

As can be seen by comparing the results for star-forming galaxies and disk-dominated galaxies with the results obtained for “all” galaxies, a significant part of the decrease in HI gas mass fraction as a function of density is driven by processes acting on star-forming, disk-dominated systems. In contrast, in the high mass bin, there is no significant decline in HI mass fraction as a function of local density for star-forming, disk-dominated galaxies. Most of the decline in HI mass fraction for massive galaxies seen in the top-right panel must thus be driven by an increase in the fraction of passive, early-type galaxies in denser environments.

It is also interesting to compare the decrease in the HI gas mass with the decrease in the central specific star formation rate measured within the fiber. The decrease in central sSFR is driven by passive, early-type galaxies in both stellar mass bins. The processes acting on atomic gas disks apparently do not affect the central sSFRs at all, at least over the range of local densities probed by our sample.

2.1 Comparison with models

So far, we have tentatively interpreted our results as possible evidence for the effect of ram-pressure acting on the atomic gas in disks in low mass galaxies in environments characteristic of galaxy groups. We do not, however, have information about the spatial distribution of the gas in our galaxies. We have made an “ansatz” that on average the gas will be more spatially extended than the star formation and that ram-pressure will more strongly affect the HI gas in the outskirts of galaxies than the star-forming (i.e. molecular) gas.

In this section, we compare our data with results from semi-analytic models where ram-pressure stripping of the cold interstellar medium of galaxies is *not taken into account*. We show that these models predict relative trends in cold gas mass fractions and specific star formation rates that do not agree with the observations.

We make use of outputs from the semi-

analytic models of Guo et al. (2011, hereafter Guo11) implemented on the Millennium II simulation, which are publically available for download at <http://www.mpa-garching.mpg.de/galform/millennium-II/>.

In these models, the cold interstellar medium of a galaxy is distributed in a disk with size that scales as the product of the virial radius and the spin parameter of its host halo. Cold gas is supplied both by infall of diffuse gas and by gas from accreted satellites. Cold gas is depleted by star formation and reheated to the hot phase by supernovae. The total star formation rate in the disk scales with its total cold gas content following a simplified version of the Kennicutt (1998) law. Stars will not form in a disk unless the total cold gas mass exceeds a certain critical value, which is set by the condition that its surface density is large enough for the gas to be gravitationally unstable (Toomre 1964). In the model, this stability criterion is a global rather than a local one.

Tidal effects, ram-pressure stripping and radio AGN feedback act on the *diffuse gas* associated with each galaxy and prevent it from cooling, condensing and forming new stars. As shown in Figure 3 of Guo11, the implementation of these quenching processes in the models lead to trends in the fraction of actively star forming galaxies as a function of projected distance from the centres of rich clusters that are in relatively good agreement with observations.

We make use of a set of 100 mock SDSS galaxy catalogues from the Guo11 model that match both the sky mask and the magnitude and redshift limits of the SDSS DR7 sample. These are the same mock catalogues that were used for interpreting SDSS data in a recent paper by Li et al. (2012). Detailed description of the methodology for constructing the mocks can be found in Li et al. (2006b; 2007).

We begin by extracting a volume from each mock catalogue that is exactly matched in redshift and sky area coverage to ALFALFA *sample A*. We select galaxies with $\text{Log } M_{\star} [M_{\odot}] = [10; 11.5]$, and then apply the same method used for the observations to compute a local density parameter (N) by counting the neighbours more massive than $M_{\star} = 10^{9.5} M_{\odot}$ inside a cylinder of 1 Mpc radius and depth $\pm 500 \text{ km s}^{-1}$.

In Figure 5, we compare the fractions of quenched objects, defined as galaxies with $\text{SFR}/M_{\star} \leq 10^{-11.2} \text{ yr}^{-1}$, in the real sample and in the mock catalogues. Results are shown for two stellar mass bins and we normalize the quenched fraction N_q/N in each density bin to the value for isolated objects with $N = 0$. Red lines show results for the real data and black dotted lines are for the model galaxies. The error bars on the data are obtained by boot-strap resampling. For the models, the error bars represent the variance over the 100 mock catalogues. As can be seen, the models and the data agree quite well. The fraction of quenched low mass galaxies is somewhat higher in the data than in the models in the highest density bin ($N > 10$), where the disagreement is at about 2σ level.

As we have discussed, in the models there are a variety of processes that quench star formation in galaxies. Feedback from radio AGN acts to prevent gas from cooling onto the *central galaxies* of dark matter halos, whereas tidal effects and ram-pressure stripping of the hot gas will affect ongoing star formation in *satellite galaxies*.

In Figure 6, black curves show the fraction of model galaxies of given stellar mass that are satellites as a func-

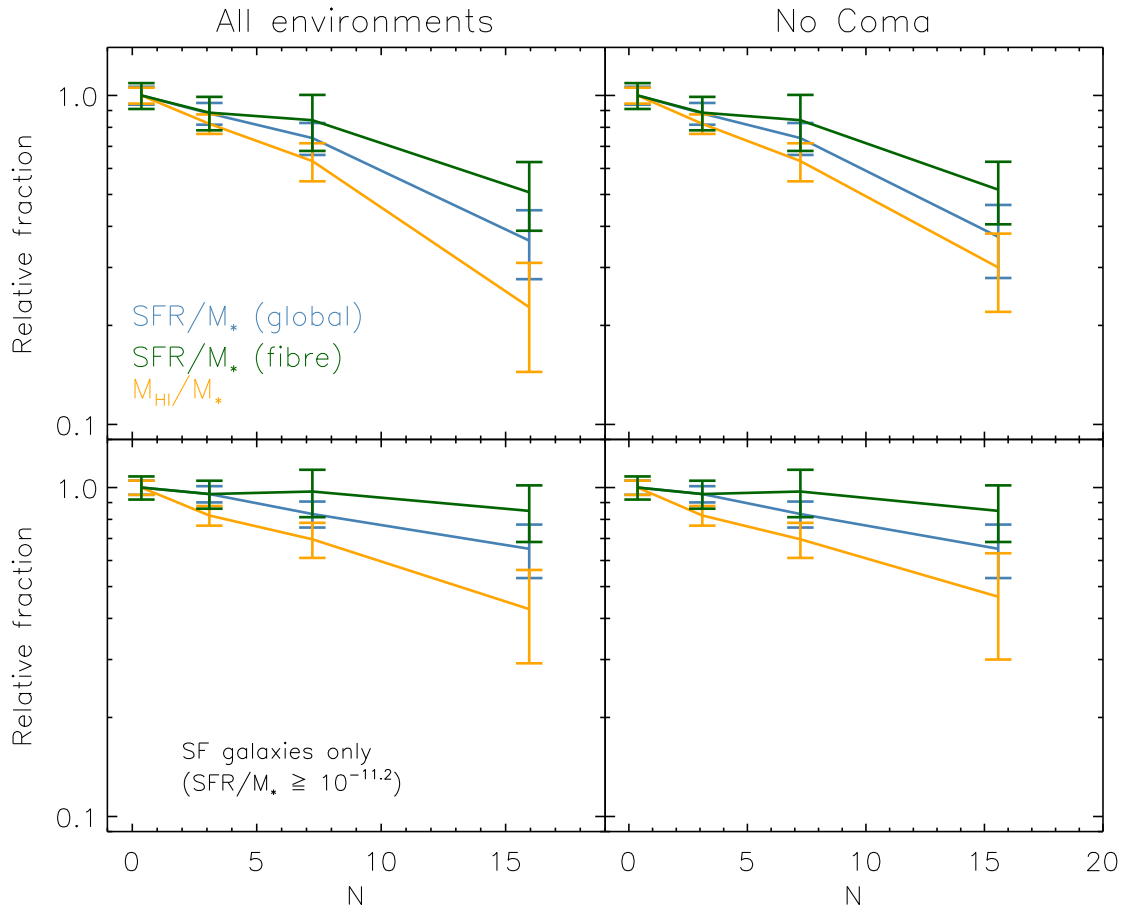


Figure 4. The relative dependence of HI gas fraction (orange), the global specific star formation rate (blue) and the fibre specific star formation rate (green) as a function of local density for galaxies with $10 < \text{Log } M_{\star} < 10.5$. The left panels show results for galaxies in *sample A*, all (top) or only the star forming ones (bottom); the right panels show analogous results when galaxies in the vicinity of the Coma cluster are removed.

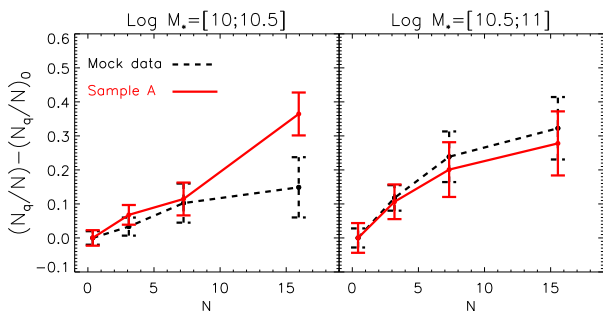


Figure 5. Comparison of the density dependence of the fraction of “quenched” galaxies with $\text{SFR}/M_{\star} \leq 10^{-11.2} \text{ yr}^{-1}$ in the data (solid red lines) and in the mock catalogues (dashed black). We plot the fraction of quenched objects with respect to that found for isolated objects: $(N_q/N) - (N_q/N)_0$. The two different panels show results for two different stellar mass bins, as reported on top.

tion of the density parameter N . As can be seen, in the lower stellar mass bin ($10 < \text{Log } M_{\star} < 10.5$), the fraction of satellite galaxies increases very strongly as a function of N . For $N = 5$, 60 percent of galaxies are satellites and for $N > 10$,

the fraction of satellites is around 0.9. This means that the analysis of the full sample of low mass galaxies in this paper is likely to probe the physical processes relevant to satellite rather than to central galaxies. In the higher stellar mass bin ($10.5 < \text{Log } M_{\star} < 11$), the fraction of satellites at intermediate values of N is smaller. However, for $N > 10$, the fraction of satellite systems still reaches values greater than 0.8.

Green and blue curves show satellite fractions as a function of local density for disk-dominated and star-forming galaxies, respectively. The satellite fractions for disk-dominated galaxies are almost the same as for the whole sample. However, for star-forming galaxies, satellite fractions are much lower. In fact, in the models, the star-forming galaxy samples are dominated by central galaxies at all densities, so such samples may not be efficient probes of tidal and ram-pressure stripping processes.

We now study relative trends in cold gas mass fraction and specific star formation rate in the models, and compare these to what is seen in the data. In Figure 3, orange and blue dashed lines show the cold gas fractions and global specific star formation rates of the model galaxies as a function of density parameter N . As can be seen, the main result is

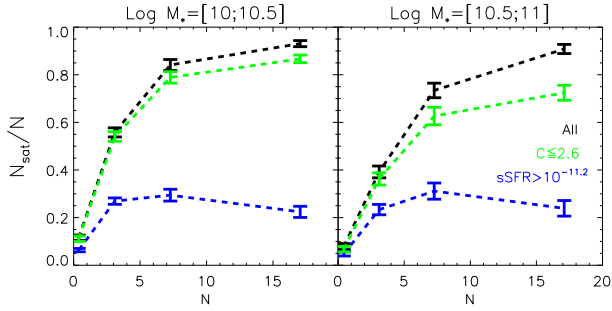


Figure 6. The mock catalogues generated from the semi-analytic models are used to calculate the fraction of galaxies of given stellar mass that are satellite systems as a function of density parameter N . Black curves show results for all galaxies in the mass bin, green curves show results for disk-dominated galaxies, and blue curves show results for star-forming galaxies. The error bars indicate the variance in the satellite fraction estimated from the 100 mock catalogues.

that the specific star formation rate decreases more strongly as a function of local density than the cold gas mass fraction. This is seen in both stellar mass bins. The effect is very strong in the top and bottom panels, which show results for all galaxies and for disk galaxies selected according to their bulge-to-disk ratios. The effect becomes considerably weaker if the sample is restricted to galaxies with ongoing star formation (middle panel), because these are mainly central galaxies³.

In the models, ram-pressure acts only on the diffuse gas halo surrounding satellites. One might think that this would imply that star formation and the cold gas remain closely coupled. The apparently puzzling result that the star formation (dashed blue line) is more strongly affected by environment than the cold gas (dashed orange) is a consequence of the fact that in galaxies where the cold gas mass has fallen below the threshold value, star formation shuts down and cold gas is no longer consumed.

In Figure 7, we compare the relations between gas mass fraction versus global specific star formation rate for model galaxies (black dotted) and *sample A* galaxies (red solid) found in rich environments ($N \geq 7$) where satellite galaxies dominate. We remind the reader that *sample A* gas fractions are estimated using stacked spectra and errors are computed via bootstrapping. For the models, we plot the mean HI gas mass fraction and the errors represent the variance between the 100 mock catalogues. As can be seen, the relation between gas fraction and specific star formation rate is much steeper in the real data than in the models (the red triangle indicates an upper limit). In the real Universe, satellite galaxies are not usually left with an inert reservoir of low-density cold gas unable to form stars. We suggest that this

³ We note that the models do not include molecular gas as a separate phase. The average molecular-to-atomic ratio in present day galaxies is about a third (Saintonge et al. 2011). If the atomic gas fraction is observed to drop by a factor to 0.5 of its field value and the molecular gas is unaffected, the total cold gas mass fraction will drop two-thirds of its field value. Accounting for the molecular component will not, however, cause a reversal in the trend between cold gas fraction and specific star formation rate.

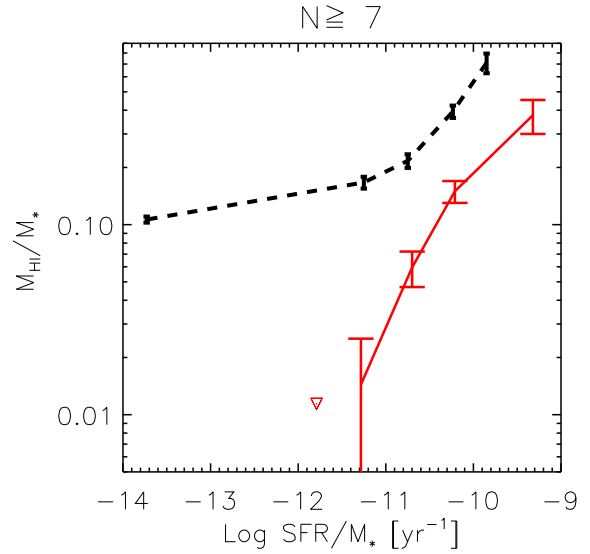


Figure 7. The relation between HI/cold gas mass fraction and global specific star formation rate for model galaxies (dashed black) and for galaxies in *sample A* (solid red) located in environments with $N \geq 7$.

is because such reservoirs are more easily stripped from the galaxy than currently assumed in the models.

In summary, the implementation of star formation quenching processes in the semi-analytic models produces relative trends in gas mass fraction and specific star formation rate that disagree with observations.

3 SUMMARY AND DISCUSSION

In this work, we have used a complete, volume-limited sample of nearby galaxies with $M_* > 10^{10} M_\odot$, with coverage by the ALFALFA, SDSS and GALEX surveys, to study how the average HI content and the global and central specific star formation rates of galaxies depend on local density at fixed stellar mass.

Our main new result is that HI gas mass fraction and specific star formation rate do not scale with local density in the same way. For galaxies with stellar masses less than $10^{10.5} M_\odot$ the atomic gas mass fractions decline most strongly as a function of density, followed by their global and central specific star formation rates. The same ordering is not seen for more massive galaxies.

In order to interpret this result, we compare our results with mock galaxy catalogues generated using the semi-analytic recipes of Guo et al. (2011) implemented on high resolution cosmological simulations of structure formation in a Λ CDM Universe. We demonstrate that the local density parameter that we have defined is tightly correlated with the fraction of galaxies that are *satellite* rather than central galaxies.

In the Guo11 models, star formation in satellite galaxies shuts down as a result of gas “starvation” – tidal and ram-pressure forces remove the gaseous halos surrounding the satellites, and as a result, cooling and infall of new gas onto these systems ceases. The star formation rates in satellites

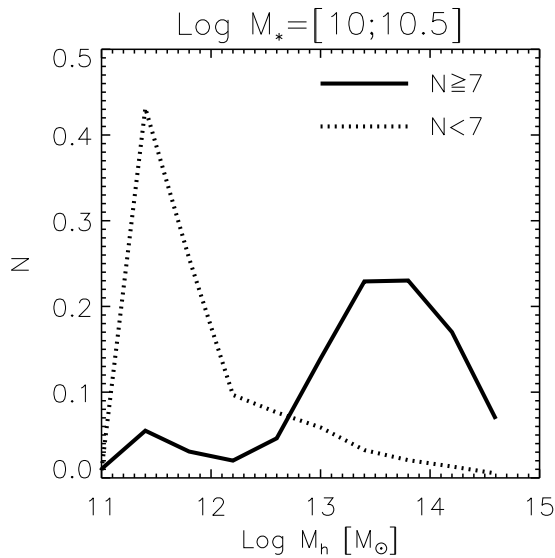


Figure 8. The distribution of dark matter halo masses that host galaxies in our mock catalogue with stellar masses in the range $10 < \log M_* < 10.5$ and local environment parameter $N > 7$ (solid curve) and $N < 7$ (dotted curve).

decline as their cold gas reservoir is used up. Eventually the surface density of cold gas falls below the critical threshold value for star formation to occur, and star formation stops entirely. The models thus predict that the average specific star formation rates of galaxies should decrease with N more strongly than their H α gas mass fractions, which is exactly the opposite to what is seen in observations.

We suggest that the assumption in the models that ram-pressure acts *only* on the diffuse gas surrounding galaxies is wrong. A question one might ask is whether the H α -deficient galaxies in our sample are located in environments where ram-pressure stripping could plausibly occur. In Figure 8, we plot the distribution of dark matter halo masses that host galaxies in our mock catalogue with stellar masses in the range $10 < \log M_* < 10.5$ and local environment parameter $N \geq 7$ (solid curve) and $N < 7$ (dotted curve). $N \geq 7$ corresponds to environments where the mean gas mass fraction of galaxies of this mass bin has dropped by more than a factor of two with respect to “isolated” galaxies with $N = 0$. As can be seen, the majority of such galaxies are in dark matter halos with masses in the range $10^{13} - 10^{14} M_\odot$, i.e. they are in galaxy *groups* rather than clusters. In contrast, most galaxies in the same stellar mass range with $N < 7$ are located in dark matter halos with masses less than $10^{12} M_\odot$, which are not expected to have a hot gas atmosphere (Birnbom & Dekel 2003). We conclude, therefore, that in order to bring the models into agreement with observations, ram-pressure effects would need to strip atomic gas from galaxies in dark matter halos more massive than $10^{13} M_\odot$.

One might ask whether tidal forces are likely to be more effective than ram-pressure at stripping material from galaxies in lower density environments. Tidal interactions between galaxies can affect both the gas and the stars in these systems. The tidal force scales as M/d^3 , where M is the mass of the neighbouring galaxy and d is its separation. In Figure 9 (top panel), we analyse trends in H α gas mass

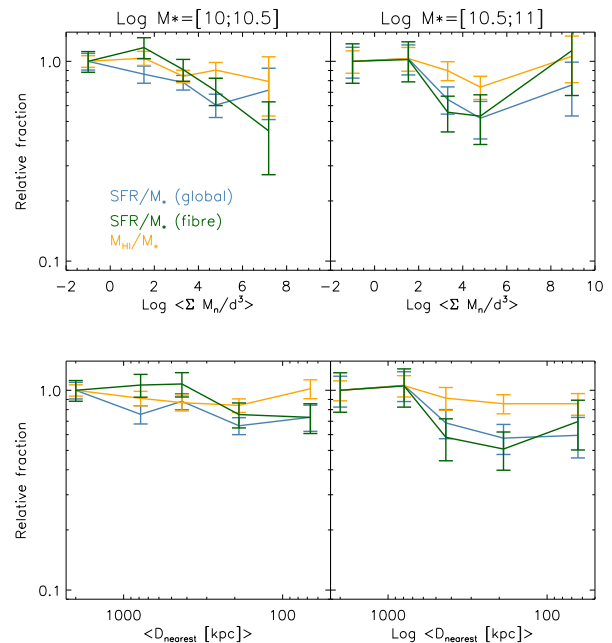


Figure 9. Comparison of the relative dependence of the H α gas fraction (orange), the global specific star formation rate (blue) and the fibre specific star formation rate (green) as a function of the summed tidal force from the surrounding galaxies (top panel) and as a function of the distance to the nearest neighbour (bottom panel). The distances are 2-D projected ones. The left and right columns correspond to the 2 bins of M_* as labelled at the top of the diagram. Error bars are evaluated by bootstrap re-sampling the galaxies in the stack.

fraction and specific star formation rate as a function of the summed tidal force from the surrounding galaxies. We use the projected distance as the measure of galaxy separation – this is not strictly correct, but it is a better indicator of true separation than a 3-dimensional estimate in rich groups and clusters where galaxy peculiar velocities are large. We also look at trends in H α gas fraction and sSFR as a function of the distance to the nearest neighbour (Figure 9, bottom panel). We find very weak effects as a function of both quantities. In addition, we do not observe the same ordering of H α gas mass fraction, global and fibre specific star formation rate seen in Figure 3 when we plot these quantities as a function of the summed tidal force. However, we note that the relevant tidal force is not the current one, at the current separation, but the maximum tidal force, experienced at the closest separation, which generally occurred in the past. Further investigation will be necessary to make conclusive statements as to the role of tidal stripping in producing the effects that we see.

We also caution that the analysis presented in this work is only statistical in nature. When stacking, it is not possible to distinguish between the effects of starvation or ram-pressure mechanisms in individual galaxies. Without resolved gas maps, we have no information on the spatial extent or the morphology of the atomic gas in the galaxies in our sample, which would more clearly diagnose ram-pressure stripping in individual systems. It would also be very interesting to study relative trends in gas and stars not only as a function of local density, but as a function of dark matter

halo mass. This could be done by correlating the available ALFALFA data with group catalogues generated from the SDSS (Yang et al. 2007). With the full ALFALFA data set, it will be possible to measure the decrease in HI for increasing group/clustercentric distance, which would put stronger constraints on ram-pressure stripping mechanisms. Eventually, the all-sky surveys planned at the Westerbork telescope (APERTIF; Verheijen et al. 2008) and at the Australian SKA Pathfinder telescope (ASKAP) will scan the sky in the 21 centimeter line with much better sensitivity and resolution than currently possible and produce datasets that are ideal for studying the environmentally-driven processes that are important in understanding galaxy evolution.

APPENDIX A: CORRECTION FOR BEAM CONFUSION

The Arecibo telescope is a single dish of 305m in diameter and has a FWHM beam of ~ 3.5 arcminutes at 21 cm, which corresponds to a physical scale of 150 kpc at the mean redshift of the galaxies in our sample ($z \simeq 0.037$). Confusion of signals coming from different galaxies within the beam at similar redshift is thus of possible concern. An example of such a case is shown in Figure A1, where two additional companion galaxies are located within the beam. The SDSS image of the galaxy is shown on the left and the yellow circle indicates the Arecibo beam size. In the right upper panel, the resulting spectrum obtained with Arecibo is shown. The vertical lines flag the expected central velocities of the three objects from their SDSS redshifts.

As discussed in Paper I, §3, we visually inspected each spectrum and discarded the ones with a strong signal close to the galaxy but not centered at the expected redshift, so the galaxy shown in A1 will actually be discarded from the sample. In our analysis, confusion will arise from the stacking of non-detected HI emission, or if the companion and main target have almost exactly the same redshift.

In previous work (Paper I, Fabello et al. 2011b) we did not apply any correction for possible confusion. For the environmental analysis, confusion may be larger, especially in the high density bins where galaxies are more clustered. In order to identify confused objects, we search the MPA-JHU spectroscopic sample of galaxies with $M_* > 3 \times 10^9 M_\odot$ for objects with projected distance smaller than the beam FWHM and velocity separation smaller than 300 km s^{-1} . If the velocity difference is larger than this value, the HI signals will not overlap. Companions at large velocity separation may increase the noise in the baseline, but do not affect the measured gas content. Around 20% of *sample A* targets have at least one companion that meet these criteria.

In order to correct for confusion, we proceed as follows:

(1) We estimate the expected gas content of each companion, using the relation between colour, stellar mass surface density and HI gas fraction derived by Zhang et al. (2009):

$$\text{Log} \left(\frac{M_{\text{HI}}}{M_*} \right) = -1.732 \cdot (g - r) + 0.215 \cdot \mu_i - 4.084, \quad (\text{A1})$$

where μ_i is the surface brightness in the i -band, and g and r are SDSS magnitudes corrected for Galactic extinction.

(2) We estimate the actual signal contaminating the stacked spectrum. First, we apply a correction factor to the

emission from the companion (f_1) using the projected distance between the target and the companion. The beam profile can be approximated with a 2D Gaussian with $\sigma_x = (2\sqrt{2} \cdot \ln 2)^{-1} \times 3.3 \text{ arcminutes}$ and $\sigma_y = (2\sqrt{2} \cdot \ln 2)^{-1} \times 3.8 \text{ arcminutes}$, so that its response decreases at the edges. The bigger companion in Figure A1, for example, lies at a projected distances of $x \simeq 0.4 \text{ arcminutes}$, and $y \simeq 1 \text{ arcminutes}$ from the target. Therefore, $f_1 = \exp[-0.5 \cdot (x/\sigma_x)^2 - 0.5 \cdot (y/\sigma_y)^2] = 0.8$ of its flux would be recorded.

Likewise, only part of the signal from the companions will actually overlap with the main target in velocity space. To estimate this second correction factor (f_2), we calculate the expected HI line widths of both the main target (w_t) and the companion (w_c), assuming a box-shape profile. To evaluate the observed width we use a Tully-Fisher relation as in Paper I (§3.2), where: $w_{obs} = w_{TF} \cdot \sin(incl)$, and w_{TF} is evaluated following the relation from Giovanelli et al. (1997), and using the SDSS i -band magnitude, k -corrected and corrected for Galactic and internal extinction (as in equations 11 and 12 in Giovanelli et al. 1997). The correction factor f_2 is given by the velocity overlap (Δw) between w_t and w_c : $f_2 = \Delta w / w_c$. As an example, in Figure A1 (bottom spectrum) the dashed regions represent how we would have modeled the three signals contributing to the spectrum. In the example, the entire flux from the green companion contributes to the measured signal ($f_2 = 1$), because it overlaps fully with the main target emission (black region). In contrast, the pink companion contributes only a very small fraction of its emission to the signal (overlap of $f_2 = 0.06$).

(3) For companions with separation from the main target $\Delta v > 50 \text{ km s}^{-1}$, we check that the HI mass predicted using Eq. A1 lies below the ALFALFA upper limit. If above, such companions should have been flagged during visual inspection of the spectrum. Failure to detect such a companion actually implies that the Zhang et al. estimate of the HI content is too high; we then reset our estimate of the gas mass of the companion to the actual ALFALFA upper limit.

(4) Finally, we subtract the contributions from all the confused companions to the HI mass measured from the stacked spectrum, as follows.

Because of the weight we apply to the spectra of the individual galaxies, a gas fraction measured from the stacked spectrum is (Paper I, §3.3):

$$\frac{M_{\text{HI}}}{M_*} = \frac{2.356 \times 10^5}{\sum_i w_i} \sum_i \frac{D_L^2(z_i)}{(1+z_i)} \frac{S_i}{M_{*,i}} w_i, \quad (\text{A2})$$

where $D_L(z)$ is the luminosity distance, S the integrated HI flux and $w = 1/rms^2$, and i the index running over the individual galaxies. The total signal S_i is actually the real emission from the main target (S_t) plus the ones from the confused objects (S_c), weighted for the two factors described in point (2):

$$S_i = S_t + \sum_c f_{1,c} f_{2,c} S_c.$$

We can rewrite equation A2 as

$$\frac{M_{\text{HI}}}{M_*} = \left(\frac{M_{\text{HI}}}{M_*} \right)_t + \frac{2.356 \times 10^5}{\sum_i w_i} \sum_i \frac{D_L^2(z_i)}{(1+z_i)} \frac{\sum_c f_{1,c} f_{2,c} S_c}{M_{*,i}} w_i.$$

And finally, if we substitute the companions' gas fractions estimated from photometry (gf_c), as described in equation

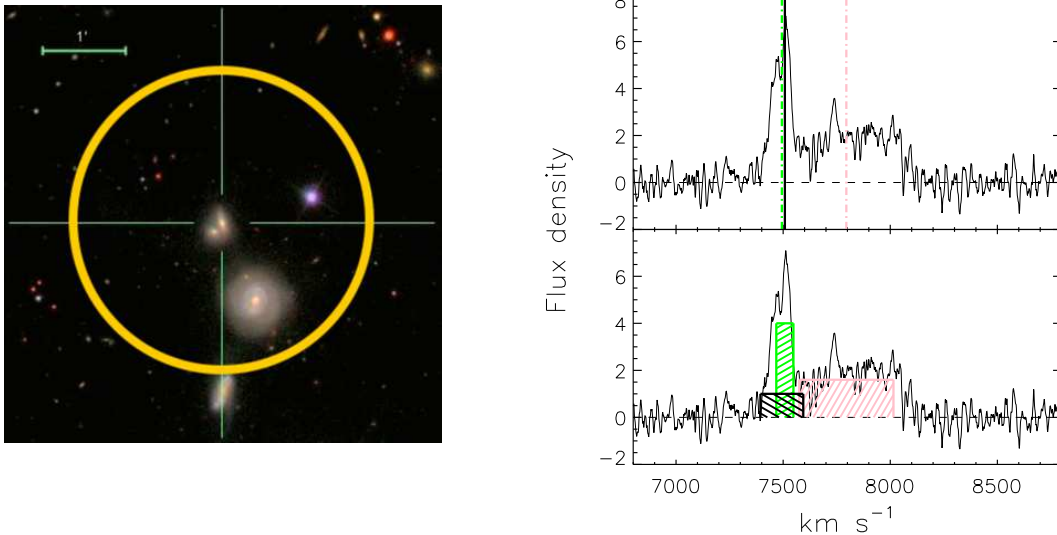


Figure A1. Example of possible signal confusion inside the Arecibo beam. *Left:* SDSS image of the galaxy GASS 49727 and its companions. The yellow circle indicates the 3.5 arcminute Arecibo beam. *Right:* the spectrum obtained with Arecibo. On top, the main target (black solid line) and the two companions (coloured dotted lines) central velocities are flagged. On the bottom, the shadowed regions show how we would model the HI signals, as described in the text.

A1, we obtain:

$$\left(\frac{M_{\text{HI}}}{M_{*}}\right)_t = \frac{M_{\text{HI}}}{M_{*}} + \frac{1}{\sum_i w_i} \sum_i \left[\frac{D_L^2(z_i)}{(1+z_i)} \frac{w_i}{M_{*,i}} \sum_c \left(\frac{f_{1;c} f_{2;c} g f_c M_{*,c} (1+z_c)}{D_L^2(z_c)} \right) \right]$$

As mentioned in the paper, confusion corrections are always small. Even in the highest density bins, the correction factor is smaller than few percent.

ACKNOWLEDGMENTS

We thank the referee of this paper, Jeff Kenney, for his helpful and constructive comments.

SF wishes to thank Luca Cortese for suggestions and useful discussions.

We thank the many members of the ALFALFA team who have contributed to the acquisition and processing of the ALFALFA dataset over the last six years.

CL is supported by NSFC (no. 11173045), Shanghai Pujiang Programme (no. 11PJ1411600), the CAS/SAFEA International Partnership Program for Creative Research Teams (KJCX2-YW-T23), the 100 Talents Program of Chinese Academy of Sciences (CAS) and the exchange program between Max Planck Society and CAS.

RG and MPH are supported by NSF grant AST-0607007 and by a grant from the Brinson Foundation.

The Arecibo Observatory is operated by SRI International under a cooperative agreement with the National Science Foundation (AST-1100968), and in alliance with Ana G. Mandez-Universidad Metropolitana, and the Universities Space Research Association.

REFERENCES

Abadi M. G., Moore B., Bower R. G., 1999, MNRAS, 308, 947

- Adelman-McCarthy, J. K., Agüeros, M. A., Allam, S. S., et al. 2008, ApJS, 175, 297
- Baldry I. K., Glazebrook K., Brinkmann J., Ivezić Ž., Lupton R. H., Nichol R. C., Szalay A. S., 2004, ApJ, 600, 681
- Balogh M., et al., 2004, MNRAS, 348, 1355
- Bamford S. P., et al., 2009, MNRAS, 393, 1324
- Birboim Y., Dekel A., 2003, MNRAS, 345, 349
- Blanton M. R., Berlind A. A., 2007, ApJ, 664, 791
- Boylan-Kolchin M., Springel V., White S. D. M., Jenkins A., Lemson G., 2009, MNRAS, 398, 1150
- Brinchmann, J., Charlot, S., White, S. D. M., et al. 2004, MNRAS, 351, 1151
- Catinella B., et al., 2010, MNRAS, 403, 683
- Cayatte V., van Gorkom J. H., Balkowski C., Kotanyi C., 1990, AJ, 100, 604
- Chabrier G., 2003, PASP, 115, 763
- Charlot, S., & Longhetti, M. 2001, MNRAS, 323, 887
- Chung, A., van Gorkom, J. H., Kenney, J. D. P., Crowl, H., & Vollmer, B. 2009, AJ, 138, 1741
- Colless M., Dunn A. M., 1996, ApJ, 458, 435
- Colless M., et al., 2001, MNRAS, 328, 1039
- Cortese, L., Catinella, B., Boissier, S., Boselli, A., & Heinis, S. 2011, MNRAS, 415, 1797
- Dressler A., 1980, ApJ, 236, 351
- Fabello S., Catinella B., Giovanelli R., Kauffmann G., Haynes M. P., Heckman T. M., Schiminovich D., 2011a, MNRAS, 411, 993
- Fabello S., Kauffmann G., Catinella B., Giovanelli R., Haynes M. P., Heckman T. M., Schiminovich D., 2011b, MNRAS, 416, 1739
- Gadotti, D. A. 2009, MNRAS, 393, 1531
- Gavazzi G., 1987, ApJ, 320, 96
- Gavazzi G., 1989, ApJ, 346, 59
- Giovanelli R., Haynes M. P., 1985, ApJ, 292, 404
- Giovanelli R., Haynes M. P., Herter T., Vogt N. P., da Costa L. N., Freudling W., Salzer J. J., Wegner G., 1997,

- AJ, 113, 53
 Giovanelli R., et al., 2005, AJ, 130, 2598
 Gunn J. E., Gott J. R., III, 1972, ApJ, 176, 1
 Guo Q., et al., 2011, MNRAS, 413, 101
 Hashimoto Y., Oemler A., Jr., Lin H., Tucker D. L., 1998, ApJ, 499, 589
 Haynes M. P., Giovanelli R., Chincarini G. L., 1984, ARA&A, 22, 445
 Haynes M. P., et al., 2011, AJ, 142, 170
 Kauffmann G., White S. D. M., Guiderdoni B., 1993, MNRAS, 264, 201
 Kauffmann G., et al., 2003, MNRAS, 341, 54
 Kauffmann G., White S. D. M., Heckman T. M., Ménard B., Brinchmann J., Charlot S., Tremonti C., Brinkmann J., 2004, MNRAS, 353, 713
 Kenney J. D. P., Young J. S., 1989, ApJ, 344, 171
 Kenney J. D. P., van Gorkom J. H., Vollmer B., 2004, AJ, 127, 3361
 Kennicutt, R. C., Roettiger, K. A., Keel, W. C., van der Hulst, J. M., & Hummel, E. 1987, NASA Conference Publication, 2466, 401
 Kennicutt R. C., Jr., 1998, ApJ, 498, 541
 Kimm T., et al., 2009, MNRAS, 394, 1131
 Larson R. B., Tinsley B. M., Caldwell C. N., 1980, ApJ, 237, 692
 Li C., Kauffmann G., Jing Y. P., White S. D. M., Börner G., Cheng F. Z., 2006a, MNRAS, 368, 21
 Li C., Kauffmann G., Wang L., White S. D. M., Heckman T. M., Jing Y. P., 2006b, MNRAS, 373, 457
 Li C., Jing Y. P., Kauffmann G., Börner G., Kang X., Wang L., 2007, MNRAS, 376, 984
 Li, C., Kauffmann, G., Heckman, T. M., Jing, Y. P., & White, S. D. M. 2008, MNRAS, 385, 1903
 Li C., Kauffmann G., Fu J., Wang J., Catinella B., Fabello S., Schiminovich D., Zhang W., 2012, arXiv, arXiv:1202.2857
 Martin, D. C., Fanson, J., Schiminovich, D., et al. 2005, ApJL, 619, L1
 Oemler A., Jr., 1974, ApJ, 194, 1
 Saintonge A., et al., 2011, MNRAS, 415, 61
 Salim S., et al., 2007, ApJS, 173, 267
 Shen S., Mo H. J., White S. D. M., Blanton M. R., Kauffmann G., Voges W., Brinkmann J., Csabai I., 2003, MNRAS, 343, 978
 Skibba R. A., et al., 2009, MNRAS, 399, 966
 Thomas D., Maraston C., Schawinski K., Sarzi M., Silk J., 2010, MNRAS, 404, 1775
 Toomre A., 1964, ApJ, 139, 1217
 van den Bosch F. C., Aquino D., Yang X., Mo H. J., Pasquali A., McIntosh D. H., Weinmann S. M., Kang X., 2008, MNRAS, 387, 79
 Verheijen, M. A. W., Oosterloo, T. A., van Cappellen, W. A., et al. 2008, The Evolution of Galaxies Through the Neutral Hydrogen Window, 1035, 265
 Vollmer, B., Braine, J., Pappalardo, C., & Hily-Blant, P. 2008, AAP, 491, 455
 Vollmer B., 2009, A&A, 502, 427
 von der Linden, A., Wild, V., Kauffmann, G., White, S. D. M., & Weinmann, S. 2010, MNRAS, 404, 1231
 Wang L., Li C., Kauffmann G., De Lucia G., 2007, MNRAS, 377, 1419
 Wang J., Overzier R., Kauffmann G., von der Linden A., Kong X., 2010, MNRAS, 401, 433
 Weinmann S. M., Kauffmann G., von der Linden A., De Lucia G., 2010, MNRAS, 406, 2249
 Weinmann, S. M., Kauffmann, G., van den Bosch, F. C., et al. 2009, MNRAS, 394, 1213
 Yang X., Mo H. J., van den Bosch F. C., Pasquali A., Li C., Barden M., 2007, ApJ, 671, 153
 York D. G., et al., 2000, AJ, 120, 1579
 Zhang W., Li C., Kauffmann G., Zou H., Catinella B., Shen S., Guo Q., Chang R., 2009, MNRAS, 397, 1243